




RESEARCH ARTICLE

Study of visible, NIR, and MIR spectroscopic properties of Er³⁺-doped tellurite glasses and glass–ceramics

Arnaud Lemiere¹  | Bartosz Bondzior^{1,2}  | Iisa Aromäki¹ | Laetitia Petit¹ 

¹Photonics Laboratory, Tampere University, Tampere, Finland

²Institute of Low Temperature and Structure Research, Polish Academy of Sciences, Wrocław, Poland

Correspondence

Arnaud Lemiere, Photonics Laboratory, Tampere University, Korkeakoulunkatu 3, Tampere 33720, Finland.
Email: arnaud.lemiere@tuni.fi

Funding information

Marie Skłodowska-Curie, Grant/Award Number: 713694; Academy of Finland, Grant/Award Numbers: 320165, 326418, 328077, 331924, 328078, 328079; Polish National Agency, Grant/Award Number: PPN/BEK/2020/1/00074

Abstract

In this paper, the structural, thermal, optical, and spectroscopic properties of Er³⁺-doped tellurite glasses with the composition 68.25TeO₂–19.5ZnO–9.75X–2.5Er₂O₃ (in mol%) with X = BaO, Na₂O, and Bi₂O₃ are reported. The glasses were prepared using the standard melt quenching method. The investigated glasses exhibit low phonon energy (~745 cm⁻¹) and low glass transition temperature varying between 300 and 350°C depending on the glass composition. The Raman spectra show a regular tellurite structure with variations in the number of bridging and non-bridging oxygens depending on the glass composition, the Na₂O and Bi₂O₃-containing glasses having the most and the least polymerized network, respectively. A thermal treatment of the glasses leads to the formation of crystals, the composition of which depends on the glass composition, as revealed by X-ray diffraction analysis and confirmed using scanning electron microscope-energy-dispersive spectroscopy. The precipitation of Er-containing crystals in the Na₂O and BaO-containing glasses leads to an increase in the intensity of the upconversion emissions. Although the Er³⁺ ions remain in the amorphous part of the Bi₂O₃-containing glass after heat treatment, it is the precipitation of Bi_{3.2}Te_{0.8}O_{6.4} crystals in this glass, which is thought to decrease the distance between the Er³⁺ ions leading to an increase in the intensity of the upconversion and mid-infrared emissions.

KEYWORDS

glass, glass–ceramic, luminescence, tellurite

1 | INTRODUCTION

New laser sources have found great interest in various fields of application, such as medicine, environmental study, sensing, or bio-engineering.^{1,2} Especially much attention is paid to the development of light sources operating between 2.0 and 5.0 μm because of the spectral signatures of molecules localized in this spectral region

that also corresponds to the transparency window of the earth's atmosphere.³ Indeed, many molecules, such as CH₄, CO₂, and OH, are absorbing at those wavelengths, and mid-infrared (MIR) laser sources could be used for air quality and monitoring applications. Light sources emitting in the visible and also in the near-infrared (NIR) regions are also of interest for applications such as optical temperature sensors,⁴ fiber amplifiers,⁵ and solid lasers.⁶

This is an open access article under the terms of the [Creative Commons Attribution-NonCommercial-NoDerivs](https://creativecommons.org/licenses/by-nc-nd/4.0/) License, which permits use and distribution in any medium, provided the original work is properly cited, the use is non-commercial and no modifications or adaptations are made.

© 2022 The Authors. *Journal of the American Ceramic Society* published by Wiley Periodicals LLC on behalf of American Ceramic Society.

Erbium ions (Er^{3+} ions) can be used to obtain emissions in the visible, NIR, and MIR when pumped at 980 nm; the NIR emission centered at 1.5 μm is due to the $^4\text{I}_{13/2} \rightarrow ^4\text{I}_{15/2}$ transition of Er^{3+} ions, whereas the MIR emission centered at 2.7 μm is achieved due to the $^4\text{I}_{11/2} \rightarrow ^4\text{I}_{13/2}$ transition. The green and red emissions centered at 530, 550, and 660 nm are due to three transitions: $^2\text{H}_{11/2} \rightarrow ^4\text{I}_{15/2}$, $^4\text{S}_{3/2} \rightarrow ^4\text{I}_{15/2}$, and $^4\text{F}_{9/2} \rightarrow ^4\text{I}_{15/2}$, respectively. The probability of radiative transition between two states strongly depends on the phonon energy of the host for the Er^{3+} ions.

Silica glass is one of the most investigated glasses due to its good optical transparency and chemical stability. However, it has low solubility of rare-earth (RE) ions.⁷ Additionally, silica and silicate glasses are known to have high phonon energy and have narrow transmission window that does not transmit light in bulks at wavelengths higher than around 3 μm .⁸ Thus, these glasses are not promising materials for applications at ~ 2.7 μm , for example. Since the last few decades, many efforts have been made in the development of other glass systems with low phonon energy such as fluorides,^{9,10} tellurites,^{11,12} chalcogenides,^{13,14} and germanates.^{15,16}

Tellurite glass system seems promising because of its wide infrared transmission window,¹² high RE solubility,¹⁷ low phonon energy, and good optical, chemical, and mechanical properties.^{12,18} The composition of the tellurite glasses can easily be modified to improve some of their properties. For example, the thermal stability of tellurite glasses can be increased by adding Na_2O or BaO as reported in Manikandan et al.¹⁹ The addition of Na_2O was also reported to open the structure of the glass,^{19,20} whereas the addition of BaO tends to make it denser and more compact.¹⁹ Er^{3+} -doped tellurite glasses have already demonstrated upconversion and the ability to produce NIR and MIR luminescence when pumped at 980 nm.^{21–23}

Glass-ceramics (GCs) are reported to be promising materials as compared to parent glasses. A GC is a glass that contains a crystalline phase and as a consequence, it combines the advantages of optical glasses and of crystal-like spectroscopic characteristics, including high absorption and emission cross sections. If the RE ions are located in a crystal with a specific crystalline phase, the GC can exhibit enhanced spectroscopic properties compared to the parent glass. To be promising, the RE-containing crystals should precipitate in volume in the glass. Additionally, the nucleation and growth of the crystals should also be controllable in order to prepare transparent GC. Zhou et al.²⁴ demonstrated a significant improvement of the upconversion properties from Er^{3+} -doped glass from the composition $70\text{TeO}_2\text{-}15\text{Li}_2\text{O-}15\text{Nb}_2\text{O}_5\text{-}0.5\text{Er}_2\text{O}_3$ (mol%) using a heat treatment at 440°C during 5 h due to the precipitation of $\text{Li}_{0.75}\text{Nb}_{1.75}\text{Te}_{0.25}\text{O}_6$ crystals. Kang et al.²⁵ also demonstrated an enhancement in the intensity of the

emission at 2.7 μm from Er^{3+} -doped $(59 - x)\text{TeO}_2\text{-}x\text{GeO}_2\text{-}8\text{TiO}_2\text{-}8\text{BaO-}22\text{Li}_2\text{O-}3\text{Er}_2\text{O}_3$ glass (with $x = 0, 10, 20, 30, 40, 50, 59$) after heat treatments between 400 and 610°C for 8 h, due to the formation of lithium- and barium-based crystals. The glass with the composition $75\text{TeO}_2\text{-}20\text{ZnO-}4\text{Na}_2\text{O-}1\text{Er}_2\text{O}_3$ (mol%) was also reported to be promising as an enhanced intensity in the luminescence at 1.55 μm was reported after a heat treatment at 450°C for 4 h due to the formation of $\text{Zn}_2\text{Te}_3\text{O}_8$ and $\text{Na}_2\text{Zn}_3(\text{CO}_3)_4 \cdot 3\text{H}_2\text{O}$ crystals.²⁶ Finally, the volume precipitation of zinc- and bismuth-based crystals was reported in the tellurite glass with the composition $70\text{TeO}_2\text{-}20\text{ZnO-}10\text{Bi}_2\text{O}_3$ during heat treatment²⁷ indicating that this glass is promising for the preparation of transparent GC.

In this context, we report the preparation and characterization of Er^{3+} -doped tellurite glasses and GCs in the $\text{TeO}_2\text{-ZnO-}\text{Na}_2\text{O}/\text{BaO}/\text{Bi}_2\text{O}_3$ system. The impact of replacing Na_2O by BaO and Bi_2O_3 on the physical, thermal, structural, optical, and spectroscopic properties is investigated. The spectroscopic properties of the glasses are measured after thermal treatment to investigate the impact of the crystallization on the spectroscopic properties of the glasses.

2 | EXPERIMENTAL PROCEDURES

Glasses with the composition $68.25\text{TeO}_2\text{-}19.5\text{ZnO-}9.75\text{X-}2.5\text{Er}_2\text{O}_3$ (in mol%) with $\text{X} = \text{BaO}, \text{Na}_2\text{O},$ and Bi_2O_3 (respectively labeled as TeBa, TeNa, and TeBi) are prepared using the standard melt-quenching method in normal atmosphere. The batches are prepared using TeO_2 (Sigma-Aldrich, 99.99%), ZnO (Sigma-Aldrich, 99.99%), BaO (Sigma-Aldrich, 99.99%), Na_2CO_3 (Sigma-Aldrich, 99.5%), Bi_2O_3 (Sigma-Aldrich, 99.99%), and Er_2O_3 (Sigma-Aldrich, 99.99%) as the raw materials. The 10-g batches are prepared and mixed using a mortar to obtain a homogeneous mixture. The mixture is transferred in a platinum (Pt) crucible and inserted into a furnace for melting for 20 min at 850°C. A step of decarbonation is realized for TeNa glass at 650°C for 30 min. The glass melt is quenched at room temperature on a brass plate and is then annealed at $\sim 40^\circ\text{C}$ below the glass transition temperature (T_g) of the glasses for 6 h to release the internal stress from the glass. Transparent orangeish glasses with no cracks are obtained. Finally, the glasses are heat treated at ($T_g + 20^\circ\text{C}$) for 17 h and then at their respective crystallization temperature T_p for 1, 6, and 12 h in order to produce GC.

The density of the glasses is measured by the Archimedes method. Ethanol was used as immersion liquid and results are obtained with an accuracy of ± 0.02 g/cm^3 .

The thermal properties of the glasses are measured using differential thermal analysis (DTA, Netzsch Jupiter

F1 instrument). The measurements were carried out in a Pt crucible using a heating rate of 10°C/min. The T_g is determined as the inflection point of the endotherm peak obtained by taking the first derivative of the DTA curve, whereas T_p is taken at the maximum of the exothermic peak. The onset of the crystallization peak, T_x , is also measured, providing information about the glass thermal stability against crystallization, $\Delta T = T_x - T_g$. All measurements are performed with an accuracy of $\pm 3^\circ\text{C}$.

The Raman spectra are acquired with a Renishaw inVia Qontor Raman microscope equipped with a cooled charge-coupled device camera using a 405 nm laser for the excitation. The spectra are normalized to the band with maximum intensity; therefore, all the changes in the band intensity are relative to the main peak. The spectra were collected from undoped glasses to avoid a strong background signal from the luminescence of Er^{3+} ions.

The absorption spectra are measured using UV-Vis-NIR spectrophotometer (UV-3600 Plus, Shimadzu) from 250 to 1800 nm. The absorption cross-section $\sigma_{\text{abs}}(\lambda)$ is calculated from absorbance using the following equation:

$$\sigma_{\text{abs}}(\lambda) = \frac{2.303 \log(I_0/I)}{L \times N_{\text{Er}^{3+}}} \quad (1)$$

where $\log(I_0/I)$ is the absorbance, L is the thickness of the sample (in cm), and $N_{\text{Er}^{3+}}$ is the concentration of RE ions in the glass (ions/cm³). The accuracy of absorption cross-section determination is $\pm 10\%$.

The spectroscopic properties of the glasses are measured from powder at room temperature using a continuous-wave 980 nm monochromatic single-mode fiber pigtailed laser diode (CM962UF76P-10R, Oclaro) for excitation. The upconversion and 1.5 μm emission spectra are acquired using a spectro 320-131 optical spectrum analyzer (Instrument Systems Optische Messtechnik GmbH, Germany). The 2.7 μm emission spectra are collected in the range of 2500–3000 nm using a monochromator coupled with an amplified MIR detector (detector PCI-4TE-4-1 \times 1, preamplifier PIP-DC-200 M-F-M4, Vigo).

An X-ray diffractometer (XRD) analyzer (PANalytical Empyrean) with Cu K_α X-ray radiation ($\lambda = 1.79 \text{ \AA}$) is used to identify the crystalline phases in the heat-treated glasses. Data are collected from $2\theta = 10^\circ$ – 60° with a step size of 0.05° .

The surface of the polished glasses prior to and after heat treatment is analyzed using a scanning electron microscope (SEM, Crossbeam 540 Carl Zeiss) equipped with an energy-dispersive spectroscopy (EDS/EDX) detector (Oxford Instruments X-MaxN 80). The samples are mounted on Al-stubs and coated with a thin carbon layer prior to the SEM/EDX analysis. The detection limit of the EDX system is $\pm 0.5 \text{ at}\%$.

3 | RESULTS AND DISCUSSION

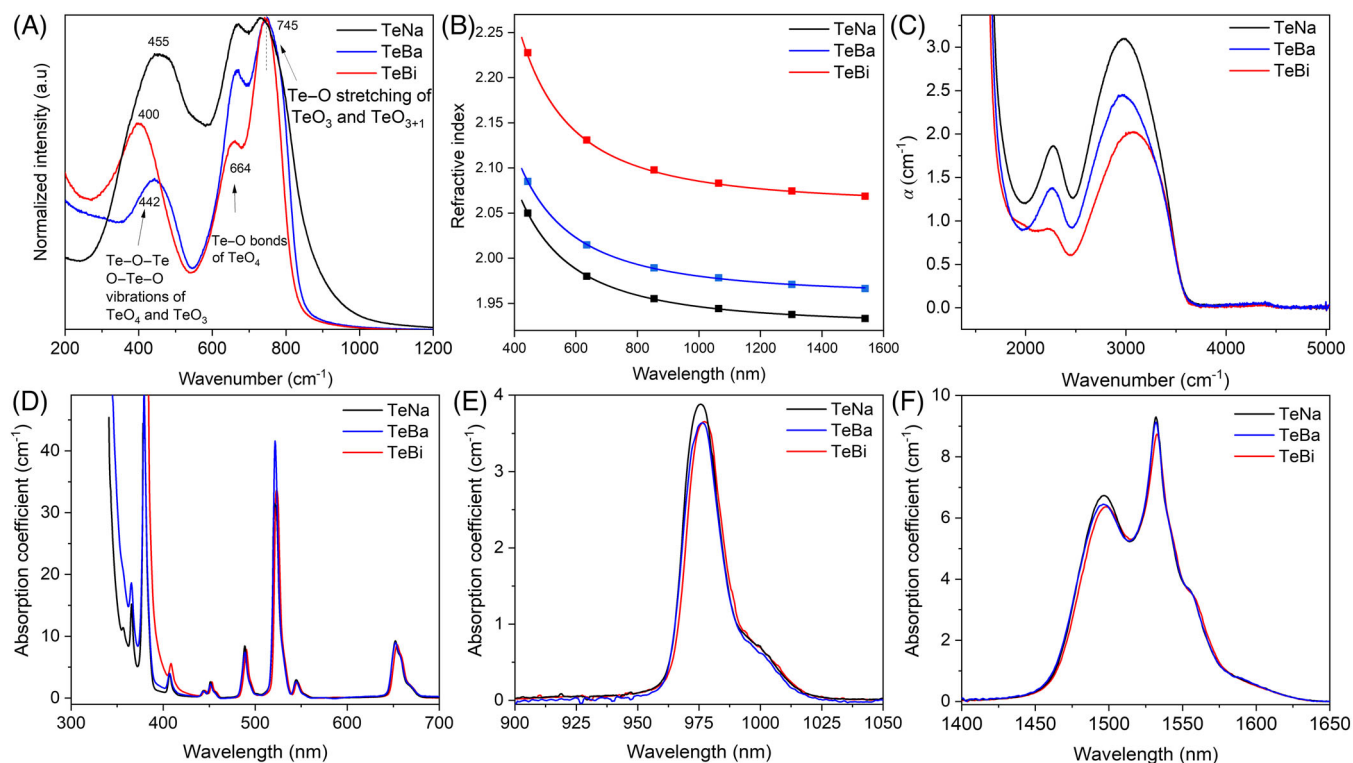
To investigate the effect of replacing Na_2O by BaO and Bi_2O_3 in the tellurite glass with the composition 68.25TeO_2 – 19.5ZnO – 9.75X – $2.5\text{Er}_2\text{O}_3$ (in mol%) with $\text{X} = \text{BaO}$, Na_2O , and Bi_2O_3 on the spectroscopic properties, the density (ρ), and molar volume (V_m) of the glasses are first measured as well as T_g , T_x , and T_p . Table 1 reports the physical and thermal properties of the glasses.

Compared to the TeNa glass, TeBa, and TeBi glasses have a higher density, which is expected because of the higher molar mass of BaO ($M_{\text{BaO}} = 153.33 \text{ g/mol}$) and Bi_2O_3 ($M_{\text{Bi}_2\text{O}_3} = 465.96 \text{ g/mol}$) compared to Na_2O ($M_{\text{Na}_2\text{O}} = 61.98 \text{ g/mol}$). Compared to the work of Massera et al.,²⁷ the density of our TeBi glass is slightly higher (6.16 g/cm^3 in Massera et al.²⁷) because of the presence of Er^{3+} in the investigated glasses. It is interesting to point out that the molar volume of the TeBi glass is high compared to that of the other glasses. This is due to the large amount of oxygen atoms in this glass that have a high ionic radius (O^{2-} : 1.40 \AA) compared to other ions (Te^{4+} : 0.97 \AA , Na^+ : 0.99 \AA , Bi^{3+} : 1.03 \AA , and Ba^{2+} : 1.35 \AA).^{28,29} The addition of BaO and Bi_2O_3 at the expense of Na_2O increases the T_g indicating a strengthening of the tellurite network. The TeBa glass can be considered a stable glass against crystallization as evidenced by its large ΔT .

As the thermal and physical properties depend on the glass composition, changes in the glass structure are expected to occur when replacing Na_2O by BaO and Bi_2O_3 . Here, the structure of the glasses was investigated using Raman spectroscopy. The normalized Raman spectra of the investigated glasses are presented in Figure 1A. The Raman spectra exhibit the typical bands for tellurite glasses centered in three different regions: 400–500, 664, and 745 cm^{-1} . One should remind that the structure of TeO_2 glass may be described in terms of a 3D network of TeO_4 trigonal bipyramid (TBP) units, in which each oxygen atom is shared by two TBP units and of TeO_3 trigonal pyramid (TP) structures, the preponderance of which is strongly dependent on the type and concentrations of network modifying oxides.³⁰ The band in the 400–500 cm^{-1} range, the position of which depends on the glass composition, is related to the Te–O–Te/O–Te–O symmetrical bending and stretching modes found at corner sharing sites of TeO_4 , TeO_3 , and TeO_{3+1} polyhedra.^{31,32} It can also be associated with Zn–O–Zn/Zn–O–Te bridges according to Manikandan et al.¹⁹ Although replacing Na_2O by BaO has a small impact on the position of this band, substituting Na_2O by Bi_2O_3 shifts this band to lower wavenumbers probably due to the formation of Te–O–Bi and Bi–O–Bi linkages as suggested in Hu et al.³³ and Bachvarova-Nedelcheva et al.³⁴ and in agreement with the large T_g of the TeBi glass as compared to that of the TeNa glass. The

TABLE 1 Physical and thermal properties of the investigated glasses. The molar volume V_m of the glasses is determined from the density ($V_m = M/\rho$)

Glass	ρ (g/cm ³) ±0.02 g/cm ³	V_m (cm ³ /mol) ±0.05 cm ³ /mol	T_g (°C) ± 3°C	T_x (°C) ± 3°C	T_p (°C) ± 3°C	$\Delta T = T_x - T_g$ (°C) ± 6°C
TeNa	5.23	26.85	307	370	440	63
TeBa	5.59	26.71	360	480	518	120
TeBi	6.24	28.81	349	418	430	69

**FIGURE 1** (A) Raman spectra (532-nm excitation), (B) refractive indices, (C) infrared (IR) absorption spectra, and absorption spectra in (D) visible, (E) at 980 nm, and (F) at 1.5 μm of the investigated glasses

band localized at 664 cm^{-1} is assigned to the symmetrical stretching vibrational modes of TeO_4 TBP, more specifically to the antisymmetric vibrations of Te–O–Te linkages among TeO_4 units.^{30,34,35} The band located at 745 cm^{-1} is attributed to the symmetrical stretching of Te–O and Te = O bonds that contain non-bridging oxygens (NBOs) in TeO_3 TP units and TeO_{3+1} polyhedra.^{30,32,33,36} The intensity of the band at 745 cm^{-1} compared to the band at 664 cm^{-1} gives information on the number of TeO_3 units compared to TeO_4 units in the network and thus on the proportion of NBOs in the glass; the higher the band at 745 cm^{-1} as compared to the band at 664 cm^{-1} , the larger concentration of NBOs.^{20,30,36,37} Substituting Na_2O by BaO and Bi_2O_3 decreases the intensity of the band at 664 cm^{-1} compared to the main band indicating a larger amount of NBOs in these glasses. Similar changes in the tellurite network when adding Na_2O to the TeO_2 – ZnO glass system was reported in Shen et al.,³⁰ the same by adding 10 mol% of

Bi_2O_3 in $x\text{Bi}_2\text{O}_3$ – $(100 - x)\text{TeO}_2$.³¹ The TeNa glass is the most polymerized glass, whereas the TeBi glass has the least polymerized network in agreement with its large V_m .

The refractive indices of the investigated glasses are shown in Figure 1B. Replacing Na_2O by BaO and Bi_2O_3 increases the refractive index as expected from the Raman spectra of the glasses. Indeed, the addition of Bi_2O_3 and BaO at the expense of Na_2O creates NBOs, which increases the refractive index as observed in Chen et al.³⁸

The FTIR spectra of the studied glasses are shown in Figure 1C. The spectra exhibit broad bands that can be related to OH groups. The shoulder at $\sim 3500\text{ cm}^{-1}$ can be related to free, weakly associated hydroxyl groups. Although Feng et al.³⁹ attributed the shoulder at 2250 cm^{-1} to strongly associated hydroxyl groups, this shoulder was related to an anharmonic contribution of the bending mode at $2\delta_{\text{OH}}$ by Guery et al.⁴⁰ It is clearly shown that the TeBi glass has the lowest amount of OH groups, whereas

TABLE 2 Optical properties of the investigated glasses

Glass	$N_{\text{Er}^{3+}} (10^{20}) / \text{ions/cm}^3 \pm 5\%$	$\alpha_{\text{abs}} (\text{cm}^{-1}) @ 980 \text{ nm}$	$\sigma_{\text{abs}} @ 980 \text{ nm} (10^{-21}) / \text{cm}^2 \pm 10\%$	$\alpha_{\text{abs}} (\text{cm}^{-1}) @ 1530 \text{ nm}$	$\sigma_{\text{abs}} @ 1530 \text{ nm} (10^{-21}) / \text{cm}^2 \pm 10\%$
TeNa	11.22	3.88	3.46	9.29	8.28
TeBa	11.27	3.63	3.22	9.13	8.11
TeBi	10.45	3.66	3.50	8.74	8.36

the TeNa glass has the largest amount of OH groups. According to Kang et al.,²⁵ the OH content can be related to the electronegativity; a large electronegativity difference between O and a cation leads to a weak covalency and to absorb more hydrogen to build OH elements. The values of electronegativity are 2.01, 1.01, 0.97, 1.67, and 3.5 eV, respectively, for Te, Na, Ba, Bi, and O.⁴¹ It is thus expected that the addition of Na^{2+} and Ba^+ will tend to build more OH elements than Bi^{3+} .

Figure 1D shows the absorption spectra of the different glasses. The typical absorption bands of Er^{3+} ions are visible, and they correspond to the 4f–4f transitions of Er^{3+} from the ground state ($^4I_{15/2}$) to the different excited states. The position of the bandgap depends on the glass composition: Due to the formation of NBOs when replacing Na_2O by BaO and Bi_2O_3 , the bandgap shifts to higher wavelength, the bandgap of the TeBi glass being located at the highest wavelength.

The shape and band positions centered at 980 and 1530 nm remain independent of the glass composition (Figure 1E,F). As seen in Table 2, the investigated glasses exhibit similar absorption cross sections at 980 and 1530 nm, indicating that the sites of Er^{3+} ions are similar in the investigated glasses. Na, Bi, and Ba are not expected to be in the coordination site of Er^{3+} ions. The absorption cross sections at 980 and 1530 nm are similar to those reported in other tellurite glasses^{42–44} and in germanate glasses⁴⁵ but are higher than in phosphate glass,⁴⁶ silica, and silicate glasses.⁴⁷

Figure 2A–C displays the normalized upconversion, NIR, and MIR spectra of the Er^{3+} -doped glasses obtained using 980-nm pumping, respectively. The upconversion spectrum is composed of three emission bands: the transition $^2H_{11/2} \rightarrow ^4I_{15/2}$ at 525 nm, $^4S_{3/2} \rightarrow ^4I_{15/2}$ at 549 nm, and $^4F_{9/2} \rightarrow ^4I_{15/2}$ at 660 nm (Figure 2A).⁴⁸ The NIR emission band corresponds to the Er^{3+} ion transition $^4I_{13/2} \rightarrow ^4I_{15/2}$ (Figure 2B)⁴⁸ and the MIR emission band to the Er^{3+} ion transition $^4I_{11/2} \rightarrow ^4I_{13/2}$ ⁴⁸ (Figure 2C). The insets in the figures display the comparison of the emission intensities, provided with an error bar of 10%. Figure 2D shows the Er^{3+} radiative transitions involved under 980 nm pumping. Except for some changes in the upconversion spectra, all glasses exhibit similar emission bands confirming that the Er^{3+} ions are located in similar sites despite the differences in glass composition. The TeBi and

TeNa glasses, respectively, exhibit the highest and lowest upconversion, NIR, and MIR emissions in agreement with their respective OH content. Indeed, energy transfer from Er^{3+} ions to quenching centers like OH^- groups is well known.⁴⁹

The glasses were heat treated at ($T_g + 20^\circ\text{C}$) for 17 h and at their crystallization peak (T_p) for 1, 6, and 12 h. All heat-treated glasses exhibit a surface crystallization: An opaque layer is formed at their surface. Figure 3A–C shows the XRD patterns of the glasses prior to and after heat treatment. The glasses show no crystallization peak prior to the heat treatment, and sharp peaks are visible in the XRD patterns after heat treatment. The XRD patterns of the TeNa and TeBa glasses exhibit the same peaks that can be assigned to the $\text{Zn}_2\text{Te}_3\text{O}_8$ crystalline phase (ICSD: 00-036-0888). Similar $\text{Zn}_2\text{Te}_3\text{O}_8$ crystal has been reported in many tellurite glasses upon thermal treatment.^{26,27,50,51} Other peaks can be seen in the XRD pattern of the heat-treated TeNa and TeBa glasses, related to $\text{Na}_2\text{Te}_4\text{O}_9$ (00-051-0441) and BaEr_2O_4 (00-042-1493), respectively. Similar Na-based crystals were found in the $(100 - x)\text{TeO}_2 - x\text{Na}_2\text{O}$ glass system with $x = 5\% - 30\%$.⁵² Other peaks can be related to Er^{3+} -based crystals, such as $\text{Er}_2(\text{TeO}_3)_3$ (00-051-0285) in the heat-treated TeNa glass and to $\text{Er}_2\text{Te}_5\text{O}_{13}$ (04-012-2914) in the heat-treated TeBa glass. Similar $\text{Er}_2\text{Te}_5\text{O}_{13}$ crystals were reported to precipitate in the $90\text{TeO}_2 - 10\text{Na}_2\text{O} - 1\text{Er}_2\text{O}_3$ glass during heat treatment.⁵³ In the XRD of the heat-treated TeBi glass, the peaks can be related to $\text{Bi}_{3.2}\text{Te}_{0.8}\text{O}_{6.4}$ (00-049-1761). $\text{Zn}_2\text{Te}_3\text{O}_8$ crystal is also suspected to precipitate in this glass. However, one should point out that no Er^{3+} -based crystal is found in the TeBi glass after heat treatment. Due to the presence of a broad diffraction background in the XRD pattern of the TeNa and TeBa glasses that can be ascribed to amorphous glass, these glasses are expected to be partially crystallized. However, the TeBi glass is expected to be the most crystallized glass as no broad diffraction background can be seen in its XRD pattern. Therefore, the addition of Bi_2O_3 at the expense of Na_2O is thought to increase the speed of crystallization. It is the decrease in the network connectivity that is thought to increase the speed of crystallization.

Figure 3D–F shows the SEM-EDS images and the composition analysis of the cross section of the glasses heat treated at ($T_g + 20^\circ\text{C}$) for 17 h and at T_p for 12 h. Te-, Na-,

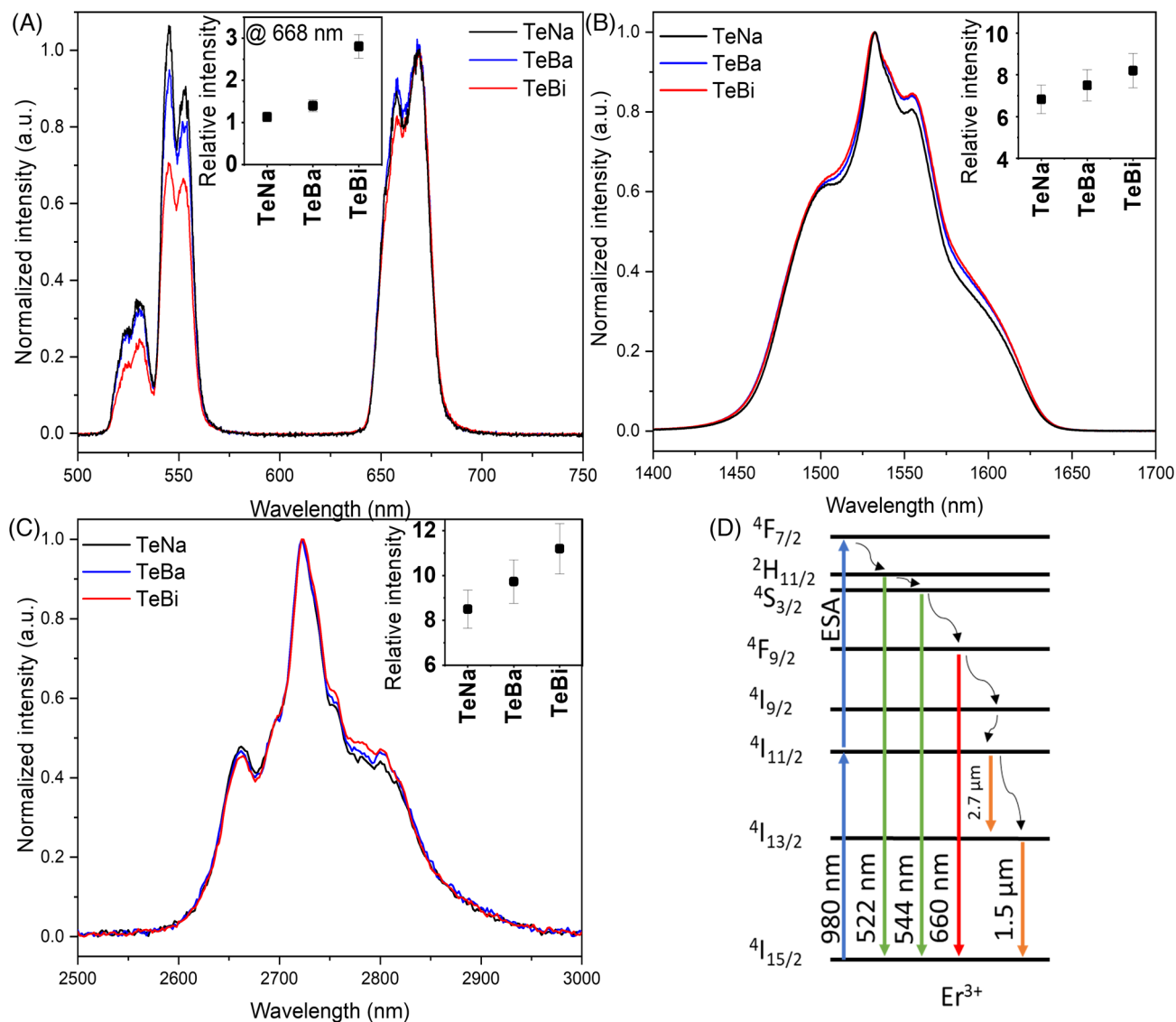


FIGURE 2 Normalized (A) upconversion, (B) 1.5- μm emission, (C) 2.7- μm emission, and (D) schematic diagram of the Er^{3+} energy levels. Insets show the intensity of the respective emissions.

Ba-, Bi-, Zn-, and Er-rich areas are visible, confirming the analysis of the XRD patterns. Although large crystals can be seen in the TeNa and TeBa glasses, the heat-treated TeBi glass is composed of small crystals ($<1 \mu\text{m}$). From the analysis of the XRD pattern and elemental mapping, it is clear that the addition of Bi_2O_3 at the expense of Na_2O , which depolymerizes the tellurite network with the creation of Te–O–Bi bonds at the expense of Te–O–Te bonds, limits the growth of large $\text{Zn}_2\text{Te}_3\text{O}_8$ crystals while promoting the crystallization of the $\text{Bi}_{3.2}\text{Te}_{0.8}\text{O}_{6.4}$ crystals.

Figure 4 shows the upconversion (A–C), the NIR (D–F), and the MIR (G–I) spectra of the glasses prior to and after heat treatment.

The heat treatment of the TeNa glass leads to a decrease in the intensity of the red and MIR emissions and to an increase in the intensity of the green emission while having

no significant impact on the intensity of the NIR emission (at $\pm 10\%$). The shape of the emission bands also changes after the thermal treatment: The bandwidth of the NIR and MIR emission bands decreases as the duration of the heat treatment increases (Figures 5), and sharp peaks appear in the green and MIR emission bands. These changes in the spectroscopic properties can be related to the precipitation of Er-containing crystals evidenced using XRD. However, as no sharp peaks can be seen in the NIR emission band, some of the Er^{3+} ions are expected to remain in the amorphous part after heat treatment, which is in agreement with the homogeneous distribution of Er seen in Figure 3D. The reduction of the bandwidth of the NIR and MIR emissions might indicate that the partial crystallization of the glass reduces the Er^{3+} site distribution in the TeNa glass.⁵⁴

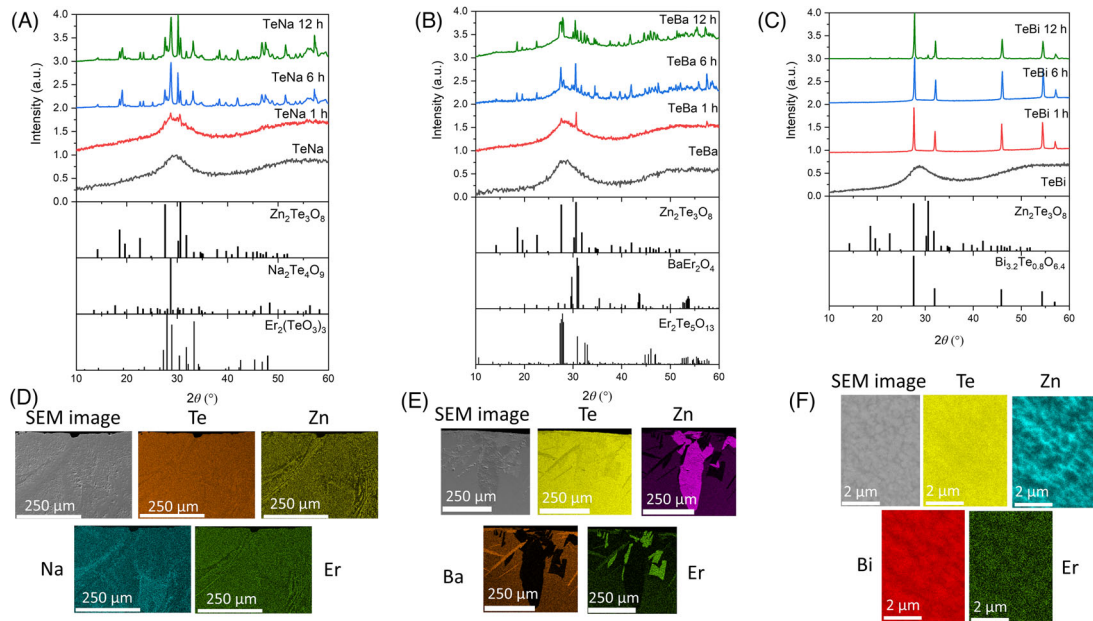


FIGURE 3 X-ray diffractometer (XRD) patterns of the (A) TeBa, (B) TeNa, (C) TeBi glasses prior to and after a heat treatment at $T_g + 20^\circ\text{C}$ for 17 h and at T_p for 1, 6, and 12 h. Scanning electron microscope energy-dispersive spectroscopy (SEM-EDS) images of the (D) TeBa, (E) TeNa, (F) TeBi glasses and the elemental mapping of the crystals in the SEM images

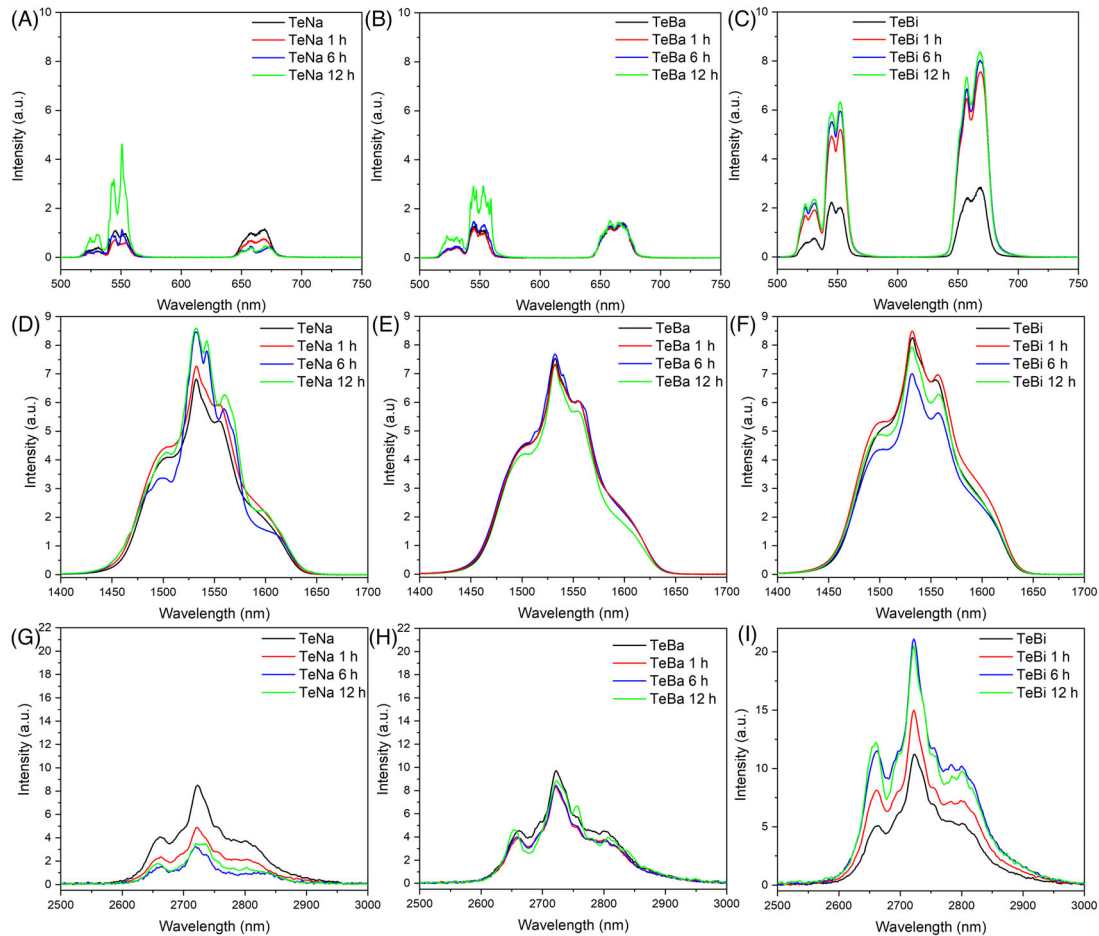


FIGURE 4 The upconversion (A–C), the near-infrared (NIR) (D–F), and the mid-infrared (MIR) (G–I) emission spectra of the glasses prior to and after heat treatment ($\lambda_{\text{exc}} = 980 \text{ nm}$)

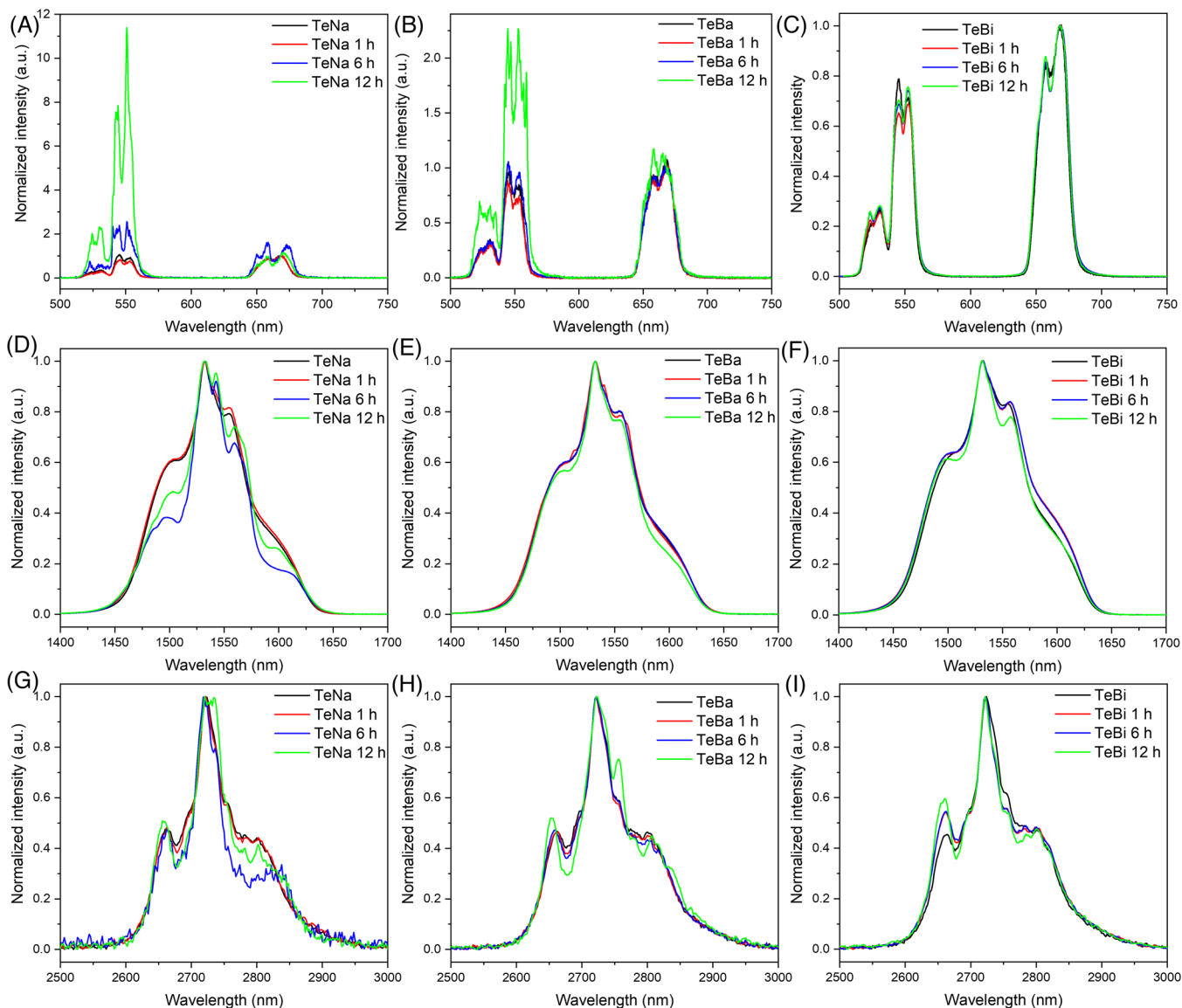


FIGURE 5 The normalized upconversion (A–C), near-infrared (NIR) (D–F), and mid-infrared (MIR) (G–I) emission spectra of the glasses prior to and after heat treatment ($\lambda_{\text{exc}} = 980 \text{ nm}$)

Similar changes in the spectroscopic properties can be seen after heat treating the TeBa glass: The changes in the green-to-red ratio and the appearance of the sharp peaks in the upconversion and MIR spectra are due to the precipitation of $\text{Er}_2\text{Te}_5\text{O}_{13}$ crystals. From the broad NIR emission band, some of the Er^{3+} ions are also expected to remain in the amorphous part. However, as opposed to TeNa glass, the bandwidth of the NIR emission band remains unchanged indicating that the site distribution of Er^{3+} ions in this glass remains similar after heat treatment. The changes in the Er^{3+} site distribution induced by the thermal treatment seem to depend on the glass network: The more polymerized network, the larger the impact of the crystallization of the Er^{3+} site distribution.

No significant changes in the shape of the upconversion, NIR, and MIR emissions can be seen for the TeBi glass after heat treatment indicating that the Er^{3+} ions are suspected to remain in the amorphous phase of the glass (Figures 4 and 5). This is in agreement with the analysis of the XRD pattern. Er^{3+} ions probably do not enter into the precipitated crystals because of the incompatible valency of Zn^{2+} and Te^{4+} compared to Er^{3+} or because of the big ionic radius of Bi^{3+} (1.03 \AA) not allowing its substitution by Er^{3+} (0.89 \AA).⁵⁵ Similarly to the TeNa glass, the heat treatment has no impact on the intensity of the NIR emission band (at $\pm 10\%$), but it increases the intensity of the upconversion and MIR emissions indicating that the Er–Er distance decreases during the thermal treatment due to

the precipitation of a large amount of crystals as discussed earlier.

4 | CONCLUSIONS


In conclusion, the impact of the replacement of Na₂O by BaO and Bi₂O₃ in tellurite glass on the spectroscopic properties and crystallization is presented. Due to the different connectivity of the glasses, the heat treatment leads to the formation of various crystals. Due to the precipitation of Er-containing crystals, the heat-treated glasses prepared with Na₂O and BaO are good candidates as green upconverters. The glass prepared with Bi₂O₃ is the most promising candidate as an upconverter and for MIR application due to the precipitation of Bi_{3.2}Te_{0.8}O_{6.4} crystals, which is expected to reduce the distance between the Er³⁺ ions.

ACKNOWLEDGMENTS

The authors would like to acknowledge the European Union's Horizon 2020 research and innovation programme under the Marie Skłodowska-Curie grant (agreement no. 713694), Academy of Finland (Flagship Programme, Photonics Research, and Innovation PREIN-320165 and Academy Projects—326418, 328077, 331924, 328078, and 328079). BB would also like to acknowledge the Polish National Agency for Academic Exchange (Bekker programme, project PPN/BEK/2020/1/00074).

ORCID

Arnaud Lemièr  <https://orcid.org/0000-0002-0852-3143>

Bartosz Bondzior  <https://orcid.org/0000-0002-1764-2427>

Laetitia Petit  <https://orcid.org/0000-0002-1673-8996>

REFERENCES

- Jackson SD. Towards high-power mid-infrared emission from a fibre laser. *Nat Photonics*. 2012;6:423–31.
- Ebendorff-Heidepriem H, Foo TC, Moore RC, Zhang W, Li Y, Monro TM, et al. Fluoride glass microstructured optical fiber with large mode area and mid-infrared transmission. *Opt Lett*. 2008;33:2861–3.
- Zhao Z, Wu B, Wang X, Pan Z, Liu Z, Zhang P, et al. Mid-infrared supercontinuum covering 2.0–16 μm in a low-loss telluride single-mode fiber. *Laser Photonics Rev*. 2017;11:1700005.
- Haouari M, Maaoui A, Saad N, Bulou A. Optical temperature sensing using green emissions of Er³⁺ doped fluoro-tellurite glass. *Sens Actuators A: Phys*. 2017;261:235–42.
- Basavapoornima Ch, Maheswari T, Depuru SR, Jayasankar CK. Sensitizing effect of Yb³⁺ ions on photoluminescence properties of Er³⁺ ions in lead phosphate glasses: optical fiber amplifiers. *Opt Mater*. 2018;86:256–69.
- Bradley JDB, M Pollnau. Erbium-doped integrated waveguide amplifiers and lasers. *Laser Photonics Rev*. 2011;5:368–403.
- Dejneka M, Samson B. Rare-earth-doped fibers for telecommunications applications. *MRS Bull*. 1999;24:39–45.
- Florence JM, Glaze FW, Hahner CH, Stair R. Transmittance of near-infrared energy by binary glasses. *J Am Ceram Soc*. 1948;31:328–31.
- Shibata S, Kanamoris T, Mitachi S, Manabe T. Preparation and characteristics of PbF₂-AlF₃ and PbF₂-ZrF₄ glasses. *Electron Commun Jpn, I: Commun*. 1980;63:94–9.
- Saad M. High purity fluoride glass synthesis: a review. In: *Laser refrigeration of solids II*. Washington: SPIE; 2009. p. 62–75.
- Redman MJ, Chen JH. Zinc tellurite glasses. *J Am Ceram Soc*. 1967;50:523–5.
- Désévéday F, Strutynski C, Lemièr A, Mathey P, Gadret G, Jules J-C, et al. Review of tellurite glasses purification issues for mid-IR optical fiber applications. *J Am Ceram Soc*. 2020;103:4017–34.
- Hilton AR. Nonoxide chalcogenide glasses as infrared optical materials. *Appl Opt*. 1966;5:1877–82.
- Singh PK, Dwivedi DK. Chalcogenide glass: fabrication techniques, properties and applications. *Ferroelectrics*. 2017;520:256–73.
- Sun KH. Contribution to refractive index and Abbe value of oxide components in glass. *J Am Ceram Soc*. 1947;30:287–9.
- Ragin T, Baranowska A, Sołtys M, Górny A, Kochanowicz M, Zmojda J, et al. Intense and wide mid-infrared luminescence in bismuth-germanate glass co-doped with Ho³⁺/Er³⁺/Yb³⁺ ions. *Infrared Phys Technol*. 2018;92:139–43.
- Wang R, Meng X, Yin F, Feng Y, Qin G, Qin W. Heavily erbium-doped low-hydroxyl fluorotellurite glasses for 2.7 μm laser applications. *Opt Mater Express*. 2013;3:1127–36.
- Zhang Y, Xia L, Li C, Ding J, Li J, Zhou X. Enhanced 2.7 μm mid-infrared emission in Er³⁺/Ho³⁺ co-doped tellurite glass. *Opt Laser Technol*. 2021;138:106913.
- Manikandan N, Rysanyanskiy A, Toulouse J. Thermal and optical properties of TeO₂-ZnO-BaO glasses. *J Non-Cryst Solids*. 2012;358:947–51.
- De Clermont-Gallerande J, Saito S, Colas M, Thomas P, Hayakawa T. New understanding of TeO₂-ZnO-Na₂O ternary glass system. *J Alloys Compd*. 2021;854:157072.
- Dai S, Yu C, Zhou G, Zhang J, Wang G, Hu L. Concentration quenching in erbium-doped tellurite glasses. *J Lumin*. 2006;117:39–45.
- Ma Y, Guo Y, Huang F, Hu L, Zhang J. Spectroscopic properties in Er³⁺ doped zinc- and tungsten-modified tellurite glasses for 2.7 μm laser materials. *J Lumin*. 2014;147:372–7.
- Maaoui A, Haouari M, Zaaboub Z, Fraj I, Saidi F, Ben Ouada H. Concentration effects on the optical spectroscopic properties of Er³⁺-doped TeO₂-Nb₂O₅-ZnO vitreous system. *J Alloys Compd*. 2016;663:395–406.
- Zhou G, Dai S, Yu C, Zhang J, Wang G, Wen L, et al. Enhancement of upconversion luminescence due to the formation of nanocrystals in Er³⁺-doped tellurite glasses. *Chin Opt Lett*. 2006;4:36–8.
- Kang S, Xiao X, Pan Q, Chen D, Qiu J, Dong G. Spectroscopic properties in Er³⁺-doped germanotellurite glasses and glass ceramics for mid-infrared laser materials. *Sci Rep*. 2017;7:43186.

26. Jlassi I, Elhouichet H, Hraiech S, Ferid M. Effect of heat treatment on the structural and optical properties of tellurite glasses doped erbium. *J Lumin.* 2012;132:832–40.
27. Massera J, Remond J, Musgraves J, Davis MJ, Misture S, Petit L, et al. Nucleation and growth behavior of glasses in the TeO_2 – Bi_2O_3 – ZnO glass system. *J Non-Cryst Solids.* 2010;356:2947–55.
28. Azuraida A, Halimah MK, Sidek AA, Azurahaman CAC, Iskandar SM, Ishak M, et al. Comparative studies of bismuth and barium boro-tellurite glass system: structural and optical properties. *Chalcogenide Lett.* 2015;12:497–503.
29. Çelikkbilek Ersundu M, Ersundu AE. Structure and crystallization kinetics of lithium tellurite glasses. *J Non-Cryst Solids.* 2016;453:150–7.
30. Shen SX, Jha A. Raman spectroscopic and DTA studies of TeO_2 – ZnO – Na_2O tellurite glasses. *Adv Mater Res.* 2008;39–40:159–64.
31. Gupta N, Khanna A. Glass and anti-glass phase co-existence and structural transitions in bismuth tellurite and bismuth niobium tellurite systems. *J Non-Cryst Solids.* 2018;481:594–603.
32. Manning S. A study of tellurite glasses for electro-optic optical fibre devices. Thesis. 2011. Accessed 18 January 2022. <https://digital.library.adelaide.edu.au/dspace/handle/2440/71483>
33. Hu X, Guery G, Boerstler J, Musgraves JD, Vanderveer D, Wachtel P, et al. Influence of Bi_2O_3 content on the crystallization behavior of TeO_2 – Bi_2O_3 – ZnO glass system. *J Non-Cryst Solids.* 2012;358:952–8.
34. Bachvarova-Nedelcheva A, Iordanova R, Ganey Sv, Dimitriev Y. Glass formation and structural studies of glasses in the TeO_2 – ZnO – Bi_2O_3 – Nb_2O_5 system. *J Non-Cryst Solids.* 2019;503–504:224–31.
35. Ghribi N, Dutreilh-Colas M, Ducl  re JR, Hayakawa T, Carreaud J, Karray R, et al. Thermal, optical and structural properties of glasses within the TeO_2 – TiO_2 – ZnO system. *J Alloys Compd.* 2015;622:333–40.
36. Grelowska I, Reben M, Burtan B, Sitarz M, Cisowski J, Yousef EIS, et al. Structural and optical study of tellurite–barium glasses. *J Mol Struct.* 2016;1126:219–25.
37. Aouaini F, Maaoui A, Mohamed NBH, Alanazi MM, El Maati LA. Visible to infrared down conversion of Er^{3+} doped tellurite glass for luminescent solar converters. *J Alloys Compd.* 2022;894:162506.
38. Chen Y, Nie Q, Xu T, Dai S, Wang X, Shen X. A study of nonlinear optical properties in Bi_2O_3 – WO_3 – TeO_2 glasses. *J Non-Cryst Solids.* 2008;354:3468–72.
39. Feng X, Tanabe S, Hanada T. Hydroxyl groups in erbium-doped germanotellurite glasses. *J Non-Cryst Solids.* 2001;281:48–54.
40. Guery G, Cardinal T, Fargues A, Rodriguez V, Dussauze M, Cavagnat D, et al. Influence of hydroxyl group on IR transparency of tellurite-based glasses. *Int J Appl Glass Sci.* 2014;5:178–84.
41. Little EJ, Jones MM. A complete table of electronegativities. *J Chem Educ.* 1960;37:231.
42. Nandi P, Jose G. Erbium doped phospho-tellurite glasses for 1.5 μm optical amplifiers. *Opt Commun.* 2006;265:588–93.
43. Jlassi I, Elhouichet H, Ferid M, Chtourou R, Oueslati M. Study of photoluminescence quenching in Er^{3+} -doped tellurite glasses. *Opt Mater.* 2010;32:743–7.
44. Yousef EIS. Er^{3+} ions doped tellurite glasses with high thermal stability, elasticity, absorption intensity, emission cross section and their optical application. *J Alloys Compd.* 2013;561:234–40.
45. Yang Y, Yang Z, Chen B, Li P, Li Xu, Guo Q. Spectroscopic properties and thermal stability of Er^{3+} -doped germanate–borate glasses. *J Alloys Compd.* 2009;479:883–7.
46. Ojha N, Szczodra A, Boetti NG, Massera J, Petit L. Nucleation and growth behavior of Er^{3+} doped oxyfluorophosphate glasses. *RSC Adv.* 2020;10:25703–16.
47. Barnes WL, Laming RI, Tarbox EJ, Morkel PR. Absorption and emission cross section of Er^{3+} doped silica fibers. *IEEE J Quantum Electron.* 1991;27:1004–10.
48. Lu Yu, Cai M, Cao R, Qian S, Xu S, Zhang J. Er^{3+} doped germanate–tellurite glass for mid-infrared 2.7 μm fiber laser material. *J Quant Spectrosc Radiat Transfer.* 2016;171:73–81.
49. Yan Y, Faber AJ, De Waal H. Luminescence quenching by OH groups in highly Er-doped phosphate glasses. *J Non-Cryst Solids.* 1995;181:283–90.
50. B  rger H, Kneipp K, Hobert H, Vogel W, Kozhukharov V, Neov S. Glass formation, properties and structure of glasses in the TeO_2 – ZnO system. *J Non-Cryst Solids.* 1992;151:134–42.
51. Lindolfo Da Silva LN, Torquato A, Nunes De Assis I, Dousti MR. Spectroscopic study of Er^{3+} -doped zinc-tellurite glass and opaque glass-ceramic. *Solid State Sci.* 2021;112:106444.
52. Kavaklıođlu KB, Aydin S, Çelikkbilek M, Ersundu AE. The TeO_2 – Na_2O system: thermal behavior, structural properties, and phase equilibria. *Int J Appl Glass Sci.* 2015;6:406–18.
53. Guo Y, Huang F, Zhang J. 2.7 μm emissions in Er^{3+} -doped transparent sodium tellurite glass ceramics. In: 2013 6th IEEE/International Conference on Advanced Infocomm Technology (ICAIT). 2013. p. 47–8.
54. Bigot L, Jurdyc AM, Jacquier B, Gasca L, Bayart D. Resonant fluorescence line narrowing measurements in erbium-doped glasses for optical amplifiers. *Phys Rev B.* 2002;66:214204.
55. Shannon RD. Revised effective ionic radii and systematic studies of interatomic distances in halides and chalcogenides. *Acta Cryst A.* 1976;32:751–67.

How to cite this article: Lemiere A, Bondzior B, Arom  ki I, Petit L. Study of visible, NIR, and MIR spectroscopic properties of Er^{3+} -doped tellurite glasses and glass–ceramics. *J Am Ceram Soc.* 2022;105:7186–7195.

<https://doi.org/10.1111/jace.18649>